

# Differences between mean-field dynamics and $N$ -particle quantum dynamics as a signature of entanglement

Christoph Weiss<sup>1\*</sup> and Niklas Teichmann<sup>2</sup>

<sup>1</sup>*Laboratoire Kastler Brossel, École Normale Supérieure, Université Pierre et Marie-Curie-Paris 6, 24 rue Lhomond, CNRS, F-75231 Paris Cedex 05, France and*

<sup>2</sup>*Institut Henri Poincaré, Centre Emile Borel, 11 rue P. et M. Curie, F-75231 Paris Cedex 05, France*  
(Dated: Submitted: 27 July 2007, published 10 April 2008)

A Bose-Einstein condensate in a tilted double-well potential under the influence of time-periodic potential differences is investigated in the regime where the mean-field (Gross-Pitaevskii) dynamics become chaotic. For some parameters near stable regions, even averaging over several condensate oscillations does not remove the differences between mean-field and  $N$ -particle results. While introducing decoherence via piecewise deterministic processes reduces those differences, they are due to the emergence of mesoscopic entangled states in the chaotic regime.

PACS numbers: 03.75.Gg, 05.45.Mt, 74.50.+r

Keywords: Chaos, mesoscopic entanglement, Bose-Einstein condensation

Experimentally it is possible to generate precisely controllable double-well potentials for Bose-Einstein condensates (BECs) (Ref. [1] and references therein). A future goal for this system is the realization of mesoscopic entanglement [1]. When combined with a time-periodic potential difference between the two wells, a BEC in a double well could also be used to investigate quantum chaos [2, 3, 4, 5]. Another system which is widely used to investigate quantum chaos is the quantum delta-kicked rotor [6, 7, 8]. Research on quantum chaos includes topics like quantum signatures of chaos [9], quasi-stationary distributions [10], entanglement [11, 12] and decoherence [13].

Often, a mean-field approach within the Gross-Pitaevskii equation is applied to describe BECs. Still, there are noticeable differences between mean-field dynamics and quantum dynamics: only the latter displays the well known collapse and revival phenomenon (cf. [14]). By time-averaging over several of those oscillations, these differences usually disappear. However, preliminary results [15] for the periodically driven double-well potential indicate that even under time-average, mean-field dynamics and quantum dynamics can display qualitatively different results in the regime for which the mean-field dynamics become chaotic.

In this Letter, these differences are investigated systematically. First, the  $N$ -particle Hamiltonian is introduced for which the Gross-Pitaevskii equation corresponds to a driven nonrigid pendulum. If decoherence is implemented on the  $N$ -particle level via piecewise deterministic processes, the quantum dynamics can become qualitatively similar to the mean-field dynamics. The reason for the remaining differences between both approaches is the emergence of mesoscopic entangled states.

To describe a BEC in a double well with single-particle tunneling frequency  $\Omega$  and pair interaction energy  $2\hbar\kappa$ ,

we use the Hamiltonian in two-mode approximation [16]:

$$\hat{H} = -\frac{\hbar\Omega}{2} (\hat{a}_1\hat{a}_2^\dagger + \hat{a}_1^\dagger\hat{a}_2) + \hbar\kappa (\hat{a}_1^\dagger\hat{a}_1^\dagger\hat{a}_1\hat{a}_1 + \hat{a}_2^\dagger\hat{a}_2^\dagger\hat{a}_2\hat{a}_2) + \hbar(\mu_0 + \mu_1 \sin(\omega t)) (\hat{a}_2^\dagger\hat{a}_2 - \hat{a}_1^\dagger\hat{a}_1), \quad (1)$$

where  $\hat{a}_j^{(\dagger)}$  creates (annihilates) a boson in well  $j$ ;  $\mu_0$  models the tilt and  $\mu_1$  is the driving amplitude. Such Hamiltonians have been used for schemes of entanglement generation [17, 18]; without the periodic driving, entanglement has been investigated in BECs [19, 20]. Other applications include high precision measurements, many-body quantum coherence [21, 22] and spin systems [23].

On the level of the Gross-Pitaevskii equation for the above model, a wave function is characterized by the variables  $\theta$  and  $\phi$ , where  $\cos^2[\theta/2]$  ( $\sin^2[\theta/2]$ ) is the probability of finding the condensate in well 1 (well 2) and  $\exp(i\phi)$  is the phase between the two wells. The corresponding  $N$ -particle wave-function (“atomic coherent states” [24]) with all particles in this state reads (in an expansion in the Fock-basis  $|n, N-n\rangle$  with  $n$  atoms in well 1):

$$|\theta, \phi\rangle = \sum_{n=0}^N \binom{N}{n}^{1/2} \cos^n(\theta/2) \sin^{N-n}(\theta/2) \times e^{i(N-n)\phi} |n, N-n\rangle. \quad (2)$$

The mean-field dynamics can be mapped to that of a nonrigid pendulum [15, 25]; including periodic driving the Hamilton function reads ( $z = \cos^2(\theta/2) - \sin^2(\theta/2)$ ):

$$H_{\text{mf}} = \frac{N\kappa}{\Omega} z^2 - \sqrt{1-z^2} \cos(\phi) - 2z \left( \frac{\mu_0}{\Omega} + \frac{\mu_1}{\Omega} \sin\left(\frac{\omega}{\Omega}\tau\right) \right), \quad \tau = t\Omega. \quad (3)$$

The experimentally measurable [1] population imbalance  $z/2$  can be used to characterize the mean-field dynamics. Fig. 1 shows typical Poincaré surfaces of section. The initial parameters were chosen such that tunneling

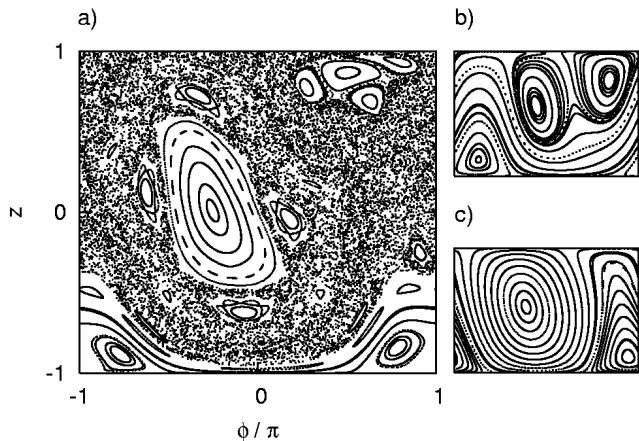


FIG. 1: Poincaré surface of section for the forced nonrigid pendulum (the mean-field dynamics (3) are plotted for various starting points at integer multiples of the oscillation period  $2\pi/\omega$ ). Closed loops are characteristic for stable orbits whereas irregular dots represent chaotic regions. For a BEC in a double-well, the parameters correspond to: (a) a tilt of  $2\mu_0/\Omega = 3.0$ , a driving frequency of  $\omega = 3\Omega$ , an interaction of  $N\kappa/\Omega = 0.8$  and a driving amplitude of  $2\mu_1/\Omega = 0.9$  (i.e. a one-“photon”-resonance [26]), (b) the 3/2-“photon”-resonance with  $N\kappa/\Omega = 0.1$ ,  $2\mu_0/\Omega = 3.0$ ,  $\omega/\Omega = 2.08$  and  $2\mu_1/\Omega = 1.8$ , (c) all parameters as in a) except for  $N\kappa/\Omega = 0.3$ .

in the driven, tilted double-well potential is enhanced by “photon”-assisted tunneling [26] (cf. Ref. [27]). If the interaction is not too low ( $N\kappa/\Omega \gtrsim 0.4 \dots 0.6$ ), regular and chaotic dynamics coexist (Fig. 1.a cf. [28]), for low interaction the dynamics are regular (Figs. 1.b and 1.c).

For the parameters corresponding to the Poincaré surface of section in Fig. 1.a, Fig. 2.a displays the differences between  $N$ -particle and mean-field dynamics by numerically calculating (using the Shampine-Gordon-routine [29]) the time-average of the (experimentally measurable [1]) population imbalance  $\langle J_z \rangle/N$  (which corresponds to the mean-field  $z/2$ ):

$$\frac{\langle J_z \rangle_T}{N} = \frac{1}{NT} \int_0^T dt \frac{1}{2} \langle \psi | \hat{a}_1^\dagger \hat{a}_1 - \hat{a}_2^\dagger \hat{a}_2 | \psi \rangle, \quad (4)$$

where for  $\langle J_z \rangle/N = \pm 0.5$  the entire condensate is in the left, respectively, right well. Each point represents an initial condition (2). The differences are small if the mean-field dynamics are regular (cf. Fig. 1.a) while they can be rather large in the chaotic regime (up to half the theoretical limit,  $\max\{|z/2 - \langle J_z \rangle/N|\} = 1$ ). Most of the deviations between  $N$ -particle dynamics and mean-field dynamics in Fig 2.a lie within twice the root-mean-square (r.m.s.)-fluctuations of the  $N$ -particle dynamics. However, contrary to the preliminary results of Ref. [15], for many initial conditions in the (classically) chaotic regime the differences can be very small; they are large near the boundaries of stable regions.

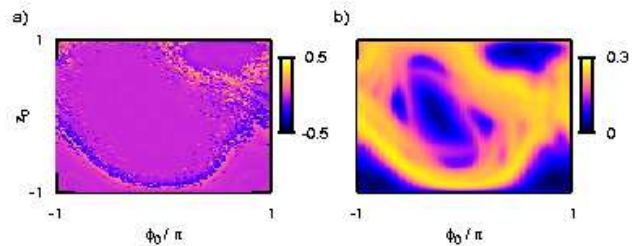


FIG. 2: (color online) Quantum dynamics ( $N = 100$ ) versus mean-field dynamics using the parameters of Fig. 1.a. (a) The difference of the time-averaged population imbalances  $\langle J_z \rangle_T/N$  and  $(z/2)_T$  as a function of  $101^2$  initial conditions  $(z_0, \phi_0)$  in a two-dimensional projection of the resulting three-dimensional plot ( $T = 100/\Omega$ ). (b) The time-averaged root-mean-square (r.m.s.)-fluctuations  $\langle \Delta J_z \rangle_T/N$  of the population imbalance as a function of the initial atomic coherent state (2).

In Fig. 2.b, the time-averaged r.m.s.-fluctuations of  $\langle J_z \rangle/N$  reproduce many features displayed in the Poincaré section in Fig. 1.a. Note that the values for the r.m.s.-fluctuations are well above those expected for  $N = 100$  particles in an atomic coherent state,  $\sin(\theta)/(2\sqrt{N}) \leq 0.05$ , thus clearly indicating that more than one atomic coherent state is involved. Bose-Einstein condensates of  $N \approx 100$  have been realized experimentally [30], both the validity of the two-mode approximation will be better and life-times of mesoscopic entangled states will be longer than in larger condensates. However, even when the calculation is repeated for  $N = 1000$  particles, the differences in the chaotic regime remain. As the (non-linear) Gross-Pitaevskii equation does not allow any superpositions, decoherence should reduce the differences between mean-field and quantum dynamics.

In this Letter, we use a piecewise deterministic process (PDP) (Ref. [31], cf. [32]) to model decoherence. To avoid to have to introduce decoherence also on the mean-field level (the atomic coherent states (2) become orthogonal in the limit  $N \rightarrow \infty$ ), we use the projection on the atomic coherent states [24]:

$$\mathbf{1} = \frac{N+1}{4\pi} \int d\theta \sin(\theta) \int d\phi |\theta, \phi\rangle \langle \theta, \phi|. \quad (5)$$

Now, the PDP simplifies to having jumps on one of the atomic coherent states (2) after time  $t$  with probability

$$p_{\text{jump}} = 1 - \exp(-\alpha t), \quad \alpha = \text{const.} > 0, \quad (6)$$

and Hamiltonian dynamics (1) between jumps. The state on which the wave-function is projected is determined by the probability distribution

$$p_{\theta, \phi} d\Omega = \frac{N+1}{4\pi} |\langle \psi | \theta, \phi \rangle|^2 \sin(\theta) d\theta d\phi. \quad (7)$$

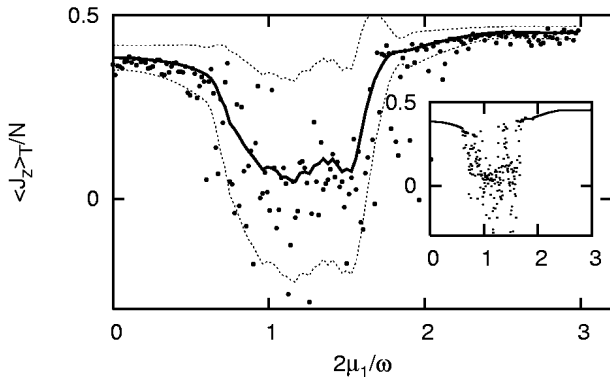


FIG. 3: Time-averaged population imbalance  $\langle J_z \rangle_T / N$  for various driving amplitudes  $\mu_1$  in a tilted driven double well ( $2\mu_0/\Omega = 3.0$ ,  $\omega = 3\Omega$ ,  $T = 100/\Omega$ ). The BEC initially is in the lower well ( $z_0 = 1$ ). Solid line:  $\langle J_z \rangle_T / N$  for  $N = 1000$  is a smooth curve as opposed to the mean-field results depicted in the inset, which display chaotic jumps for small changes of the driving amplitude. Dots in the main plot: If decoherence is included via the PDP-process described around Eq. (6) with on average  $\simeq 5$  jumps ( $\alpha = 1/20$ ) [33], the behavior is closer to the mean-field dynamics. Many dots lie in the area defined by the curves  $(\langle J_z \rangle_T \pm \langle \Delta J_z \rangle_T) / N$  (dashed lines).

Figure 3 shows that the PDP can qualitatively reproduce the results of the Gross-Pitaevskii equation [33]. Without introducing the decoherence, the qualitative difference between mean-field and quantum dynamics are quite large; averaging over several PDPs would again result in a smooth curve within the error-bars in Fig. 3. While BEC-research in quantum chaos often assumes the validity of the Gross-Pitaevskii equation [2, 3, 4, 5, 34], at least for the model investigated here, only decoherence can lead to the chaotic behavior predicted by mean field.

Furthermore, differences between quantum dynamics and mean-field dynamics can also occur in the regular regime: Fig. 4 shows that, at least for  $N = 100$ , the differences can even lie above the result for many initial conditions in the chaotic regime (Fig. 2.a). One way to reduce the differences is to average over the Husimi distribution (7) (see Fig. 4, cf. Refs. [2, 35] and references therein). This decreases the peaks of the differences between mean-field and quantum dynamics by a factor of 2 (in the chaotic regime, the factor can be of the order of 5). A perfect agreement cannot be expected as the averaged probability distribution on the mean-field level is always added whereas in quantum mechanics also destructive interference can occur.

On the level of quantum dynamics, the differences could be due to either a distribution of many atomic coherent states - or maybe even mesoscopic superpositions. For our model all mesoscopic quantum superpositions of all  $N$  particles being either in one quantum state or in another can be expressed as a sum of two atomic coherent

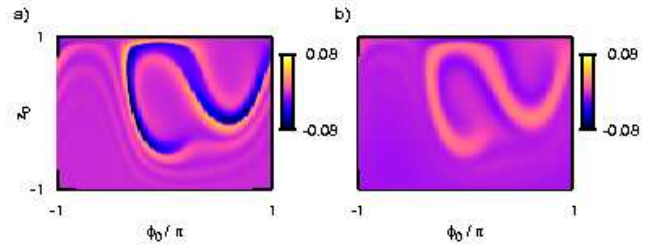


FIG. 4: (color online) Time-averaged population imbalances of quantum dynamics ( $N = 100$ ) versus mean-field dynamics at the  $3/2$ -“photon”-resonance of Fig. 1.b.

(a) The difference is plotted as a function of the initial condition  $(z_0, \phi_0)$  in a two-dimensional projection ( $T = 100/\Omega$ ). (b) As in a) but the mean-field dynamics are replaced by an average over the distribution of initial conditions (7).

states (see the explanation before Eq. (2)):

$$|\psi_{\text{sp}}\rangle = \eta (|\theta_1, \phi_1\rangle + e^{i\gamma} |\theta_2, \phi_2\rangle), \quad 0 \leq \gamma \leq 2\pi \quad (8)$$

If both parts hardly overlap,  $|\langle \theta_1, \phi_1 | \theta_2, \phi_2 \rangle| \ll 1$ , the normalization  $\eta \simeq 1/\sqrt{2}$  and  $|\psi_{\text{sp}}\rangle$  is a highly entangled mesoscopic state (for finite  $N$ , the only two orthogonal atomic coherent states (2) are  $|0, \phi_1\rangle$  and  $|\pi, \phi_2\rangle$ ). In a two-dimensional projection (cf. Fig 5.c) such a state is a bimodal distribution (for  $N \rightarrow \infty$ : two delta-peaks).

To numerically identify if a given wave-function  $|\psi\rangle$  is in a mesoscopic superposition, we start by searching the atomic coherent state  $|\theta_1, \phi_1\rangle$  for which  $|\langle \psi | \theta, \phi \rangle|^2$  reaches its maximum,  $m_1$ . Around  $(\theta_1, \phi_1)$  we define the set R1 by  $|\langle \theta, \phi | \theta_1, \phi_1 \rangle|^2 > 10^{-3}$  (cf. Fig 5.c). As both parts of the mesoscopic superposition (8) should hardly overlap, the second maximum  $m_2 = |\langle \psi | \theta_2, \phi_2 \rangle|^2$  is searched outside the set R1. The set R2 is defined analogously to R1 by  $|\langle \theta, \phi | \theta_2, \phi_2 \rangle|^2 > 10^{-3}$ . The fidelity  $|\langle \psi | \psi_{\text{sp}} \rangle|^2$  still is a function of  $\gamma$ , taking its maximum and excluding large overlaps ( $R1 \cap R2 \neq \emptyset$ ) yields:

$$p_{\text{fid}} = \begin{cases} 0 & : \text{R1 and R2 overlap} \\ \frac{1}{2} (\sqrt{m_1} + \sqrt{m_2})^2 & : \text{else} \end{cases} \quad (9)$$

Yet, this only indicates entanglement if  $p_{\text{fid}} > 0.5$ . With

$$\sigma_{\text{ent}} = \frac{m_2}{m_1} p_{\text{fid}}, \quad \sigma_{\text{ent}} \leq p_{\text{fid}} \quad (10)$$

even values of  $\sigma_{\text{ent}} \lesssim 0.5$  can identify mesoscopic superpositions (Fig. 5.c). In Fig. 5.a, the maximum value of entanglement (evaluated at  $\tau = 5$  and 10) is plotted as a function of the initial condition  $(z_0, \phi_0)$ : within the chaotic regime (left), entanglement generation happens on faster time-scales than in the regular regime (right); for longer time-scales (Fig. 5.b) the entanglement in the entire chaotic regime is more pronounced. It reaches particularly high values near initial conditions with large differences in the time-averaged population imbalances

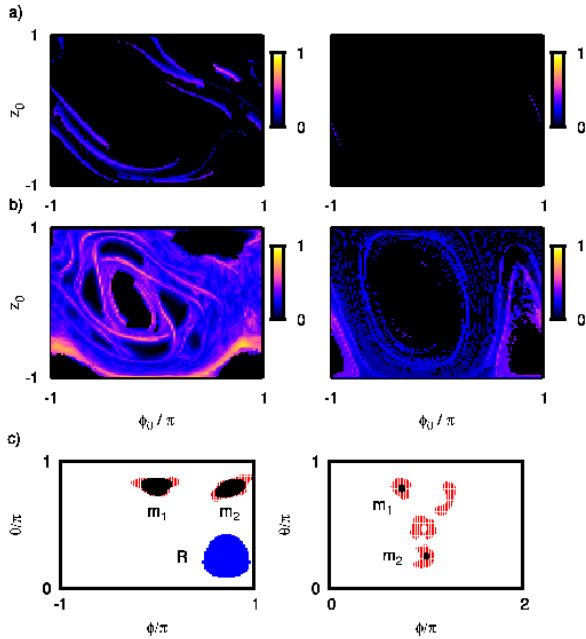


FIG. 5: (color online) Entanglement (10) for parameters as in Fig. 1.a (left column) and as in Fig. 1.c (right column). (a), (b): Mesoscopic quantum superpositions were identified at times  $\tau = 5, 10, 15, \dots$ ; the maximum value of  $\sigma_{\text{ent}}$  is displayed for  $101^2$  initial conditions  $(z_0, \phi_0)$  and for (a) short times ( $\tau = 10$ ) and (b) longer times ( $\tau = 100$ ). (c) Projection of two characteristic entangled states (with maxima  $m_1, m_2$ ) on the atomic coherent states (2). Black (grey/red) regions:  $|\langle \theta, \phi | \psi \rangle|^2 > 0.16$  ( $> 0.05$ ). Left:  $z_0 = -0.6$ ,  $\phi_0 = -2.764601535$ ,  $\tau = 80$ ,  $\sigma_{\text{ent}} \simeq 72.3\%$ . Right:  $z_0 = -0.98$ ,  $\phi_0 = -2.701769682$ ,  $\tau = 75$ ,  $\sigma_{\text{ent}} \simeq 33.5\%$ . In the left plot, the large blue/grey circle is a typical set  $R$  around  $|\tilde{\theta}, \tilde{\phi}\rangle$  with  $|\langle \theta, \phi | \tilde{\theta}, \tilde{\phi} \rangle|^2 > 0.001$  (cf. Eq. (9)).

(Fig. 2.a). We obtained qualitatively similar results also for other values of driving amplitude and interaction.

To conclude, generation of mesoscopic entangled states can be a signature of quantum chaos for a BEC in a periodically driven double well potential. We investigated the driving near multi-“photon” tunneling resonances [26] which were recently observed experimentally for a BEC in an optical lattice [36]. While decoherence can lead to a “chaotic” behavior similar to the predictions of the Gross-Pitaevskii equation, the differences between quantum dynamics and mean-field dynamics are due to the emergence of mesoscopic superpositions. If the mean-field dynamics are chaotic, the entanglement generation is accelerated and its values are enhanced.

We thank H. P. Breuer, Y. Castin, A. Eckardt and

M. Holthaus for insightful discussions. Funding by the EU is gratefully acknowledged (CW: contract MEIF-CT-2006-038407; NT: contract MEST-CT-2005-019755).

\* Electronic address: weiss@theorie.physik.uni-oldenburg.de

- [1] R. Gati and M. K. Oberthaler, *J. Phys. B* **40**, R61 (2007).
- [2] R. Utermann *et al.*, *Phys. Rev. E* **49**, 273 (1994).
- [3] F. K. Abdullaev and R. A. Kraenkel, *Phys. Rev. A* **62**, 023613 (2000).
- [4] S. Ghose *et al.*, *Phys. Rev. E* **64**, 056119 (2001).
- [5] C. Lee *et al.*, *Phys. Rev. A* **64**, 053604 (2001).
- [6] F. L. Moore *et al.*, *Phys. Rev. Lett.* **75**, 4598 (1995).
- [7] M. B. d’Arcy *et al.*, *Phys. Rev. Lett.* **87**, 074102 (2001).
- [8] C. E. Creffield *et al.*, *Phys. Rev. E* **73**, 066202 (2006).
- [9] F. Haake, *Quantum Signatures of Chaos* (Springer, Berlin, 1992).
- [10] H.-P. Breuer *et al.*, *Phys. Rev. E* **61**, 4883 (2000).
- [11] I. Garcia-Mata *et al.*, *Phys. Rev. Lett.* **98**, 120504 (2007).
- [12] S. Ghose and B. C. Sanders, *Phys. Rev. A* **70**, 062315 (2004).
- [13] D. Braun, *Dissipative Quantum Chaos and Decoherence* (Springer, Berlin, 2001).
- [14] M. Greiner *et al.*, *Nature* **419**, 51 (2002).
- [15] N. Teichmann *et al.*, *Nonlinear Phenomena in Complex Systems* **9**, 254 (2006).
- [16] H. J. Lipkin *et al.*, *Nucl. Phys.* **62**, 188 (1965); G. J. Milburn *et al.*, *Phys. Rev. A* **55**, 4318 (1997).
- [17] N. Teichmann and C. Weiss, *EPL* **78**, 10009 (2007).
- [18] C. E. Creffield, *Phys. Rev. Lett.* **99**, 110501 (2007).
- [19] A. Micheli *et al.*, *Phys. Rev. A* **67**, 013607 (2003).
- [20] K. W. Mahmud *et al.*, *J. Phys. B* **36**, L265 (2003).
- [21] C. Lee, *Phys. Rev. Lett.* **97**, 150402 (2006).
- [22] C. Lee *et al.*, *EPL* **81**, 60006 (2008).
- [23] S. Dusuel and J. Vidal, *Phys. Rev. B* **71**, 224420 (2005).
- [24] L. Mandel and E. Wolf, *Optical coherence and quantum optics* (Cambridge University Press, Cambridge, 1995).
- [25] A. Smerzi *et al.*, *Phys. Rev. Lett.* **79**, 4950 (1997).
- [26] A. Eckardt *et al.*, *Phys. Rev. Lett.* **95**, 200401 (2005).
- [27] M. Grifoni and P. Hänggi, *Phys. Rep.* **304**, 229 (1998).
- [28] J. Guckenheimer and P. Holmes, *Nonlinear Oscillations, Dynamical Systems and Bifurcations of Vector Fields* (Springer, New York, 1983).
- [29] L. F. Shampine and M. K. Gordon, *Computer Solution of Ordinary Differential Equations* (Freeman, San Francisco, 1975).
- [30] C.-S. Chuu *et al.*, *Phys. Rev. Lett.* **95**, 260403 (2005).
- [31] H.-P. Breuer and F. Petruccione, *The Theory of Open Quantum Systems* (Clarendon Press, Oxford, 2006).
- [32] J. Dalibard *et al.*, *Phys. Rev. Lett.* **68**, 580 (1992).
- [33] A higher  $\alpha$  leads to a larger statistical spread.  $\alpha$  includes the influence of the environment; it would, e.g., be larger for larger BECs.
- [34] A. D. Martin *et al.*, *Phys. Rev. Lett.* **98**, 020402 (2007).
- [35] M. P. Strzys *et al.*, *New J. Phys.* **10**, 013024 (2008).
- [36] C. Sias *et al.*, *Phys. Rev. Lett.* **100**, 040404 (2008).